· Article · Advances in Polar Science
doi: 10.12429/j.advps.2023.0102 June 2023 Vol. 34 No. 2: 80-90

Modified Circumpolar Deep Water inflow to the Dotson-Getz Trough in the summers of 2020 and 2022

XIE Chunhu[1], SHI Jiuxin[1*], SUN Yongming[1], JIANG Jindong[2], Guy D. WILLIAMS[1,2], SHUAI Hongtao[1], LIN Lijin[1], XIAO Changhao[1], CAO Yong[1] & WANG Kun[3]

[1] Physical Oceanography Laboratory, Ocean University of China, Qingdao 266100, China;
[2] Center for Ocean and Climate Research, First Institute of Oceanography, Ministry of Natural Resources, Qingdao 266061, China;
[3] College of Marine Sciences, Shanghai Ocean University, Shanghai 201306, China

Received 25 March 2023; accepted 25 April 2023; published online 30 June 2023

Abstract The melting of the West Antarctic Ice Shelf has increased since the 1990s, driven by the relatively warm Circumpolar Deep Water (CDW) that penetrates into the West Antarctic Ice Shelf cavities through submarine glacial troughs across the continental shelf. In this study, temperature, salinity, and current velocity data obtained by the Chinese National Antarctic Research Expedition in the Dotson-Getz Trough (DGT) shows clear differences in distribution of modified Circumpolar Deep Water (mCDW) in the summers of 2020 and 2022. Combined with contemporaneous wind data and additional temperature and salinity data from instrumented seals, the processes and mechanisms responsible for this variation are discussed. Compared with 2020, there is a significant increase in mCDW thickness in 2022, with a doubling of total heat content as the mCDW inflow path across the DGT shifts towards the eastern bank. We propose that a southward shift in the westerly winds in the summer of 2022 moved the upper oceanic divergence zone southward towards the continental slope, promoting the upwelling of mCDW above 500 m. Concurrently, stronger westerly winds over the continental slope strengthened the eastward undercurrent, increasing the transport of this mCDW and its associated heat content to the DGT through Ekman dynamics. These observations show there is strong interannual variability in the strength, path and extent of mCDW inflows to the DGT and that care must be taken when planning observation programs for long-term monitoring of the oceanic heat input to the ice shelves of this globally significant region.

Keywords **modified Circumpolar Deep Water**, **wind**, **Dotson-Getz Trough**, **Amundsen Sea**, **Antarctica**

Citation: Xie C H, Shi J X, Sun Y M, et al. Modified Circumpolar Deep Water inflow to the Dotson-Getz Trough in the summers of 2020 and 2022. Adv Polar Sci, 2023, 34(2): 80-90, doi: 10.12429/j.advps.2023.0102

1 Introduction

Recent studies have highlighted the Amundsen Sea as one of the world's largest regions of continental ice loss, with significant impact on global sea level rise (Joughin et al., 2014; Sutterley et al., 2014). Since 1973, the Amundsen Sea has experienced a 77% increase in ice discharge due to glacier acceleration, and as such is responsible for about 10% of current global sea level rise (Mouginot et al., 2014; Turner et al., 2017). Existing studies have concluded that the accelerated output of glaciers in the Amundsen Sea is associated with accelerated ice shelf thinning (Pritchard et al., 2012; Dutrieux et al., 2014). Relatively warm Circumpolar

* Corresponding author, ORCID: 0000-0002-5825-8894, E-mail: shijiuxin@ouc.edu.cn

Deep Water (CDW) flows onto the Amundsen Sea continental shelf and into sub-ice-shelf ocean cavities (Jenkins et al., 2010) and is thought to be responsible for the recent substantial grounding-line retreat and accelerated thinning of ice shelves (Arneborg et al., 2012; Kim et al., 2017, 2021; Dotto et al., 2019, 2020).

Nakayama et al. (2018) used a regional ocean numerical model to show that CDW flows to the Amundsen Sea continental shelf via the Southern Antarctic Circumpolar Current Front (SACCF), which is the southernmost tributary of the Antarctic Circumpolar Current (ACC). Warm and saline CDW (θ>1.5 °C, S>34.5) mainly flows onto the Amundsen Sea continental shelf along submarine glacial troughs (Kim et al., 2017; Dotto et al., 2019, 2020), mixing with local, cooler shelf water to form modified Circumpolar Deep Water (mCDW, θ>0 °C, S>34.4). In contrast to the warm, but saline mCDW at the bottom, the upper layer is occupied by Winter Water (WW, θ<−1.5 °C, S≈34.2), which is the cooler and fresher remnant of the previous winter mixed layer formed by brine rejection during sea ice growth. The surface layer above the WW is the Antarctic Summer Surface Water (AASSW), which is largely the summer mixed layer that is warmer and fresher due to solar heating and sea ice melting.

Previous observations of the circulation in the Dotson-Getz Trough (DGT), located in the western part of the Amundsen Sea (Figure 1), indicate that mCDW is mainly transported southward along the eastern flank of the DGT (Walker et al., 2007; Wåhlin et al., 2010; Arneborg et al., 2012), and that while the transport pattern is continuous and stable, its flux has seasonal variations (Arneborg et al., 2012). The inflow of mCDW within the DGT peaks in late summer and is weakest in late winter (Wåhlin et al., 2010; Arneborg et al., 2012; Kim et al., 2017). The seasonal variation of mCDW at the bottom of the continental shelf is thought to be primarily due to the seasonal variation in wind (Kim et al., 2017). Arneborg et al. (2012) indicated that interannual variability of mCDW also exists at the bottom of the continental shelf and suggested that the interannual variation is greater than the seasonal variation. Many studies have suggested that the variation of mCDW on the Amundsen Sea continental shelf is related to the variation of wind speed and direction (Dotto et al., 2019), such that when the westerly winds move south and strengthen, a larger amount of mCDW flows onto the continental shelf (Thoma et al., 2008; Dotto et al., 2020).

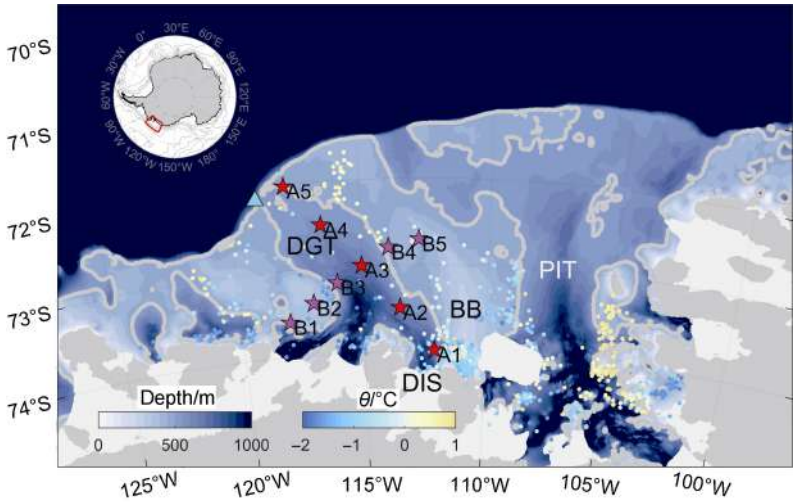

Figure 1 The study area in the Amundsen Sea with conductivity-temperature-depth (CTD) locations and bottom temperature from instrumented seal data. Key bathymetric features include Dotson-Getz Trough (DGT) and Pine Island Trough (PIT), respectively. Bear Bank (BB) and Dotson Ice Shelf (DIS) are indicated. Bathymetry (gray shade) is from RTopo2 (500 m isobath is depicted by grey contours). The red and pink stars represent the position of the ship-based CTD stations. The cyan triangles represent the position of XBT stations. The colored dots represent bottom temperature from seal CTD.

The variation of the eastward undercurrent on the Amundsen Sea continental slope can also regulate the inflow of mCDW to the continental shelf. Previous studies suggest that the eastward undercurrent currents on the slope can transport mCDW to the continental shelf by advection (St-Laurent et al., 2013; Walker et al., 2013) or bottom Ekman dynamics (Wåhlin et al., 2012) when they encounter the trough. Dotto et al. (2019) divided the inflow pattern of mCDW in the Amundsen Sea into eastern and western pathways. The PIT, which is located in the eastern part of the Amundsen Sea, has a deeper entrance at the shelf break where the upper boundary of the CDW is shallower, promoting flow onto the eastern shelf of the Amundsen Sea. The DGT on the western shelf is relatively shallow at the shelf break, where the upper boundary of the CDW is relatively deep, reducing the flow of CDW onto the shelf compared to the eastern trough (Dotto et al., 2019). It is only when the eastward undercurrent strengthens that the flow of mCDW into the trough becomes significant. Therefore, the proportion of mCDW in the western part of

the shelf is smaller than in the eastern part, and there is large interannual variability (Dotto et al., 2019).

Existing studies have focused on the PIT and provided greater understanding of the mCDW inflow mechanisms in this region. While attention to the western DGT has increased in recent years, the understanding of the inflow mechanisms of mCDW in this region is still unclear. The Chinese National Antarctic Research Expedition (CHINARE) conducted hydrographic observations in the DGT during the summers of 2020 and 2022, obtaining repeat observations of temperature, salinity, and current data. In this paper, these data are combined with instrumented seal data (salinity and temperature) and a wind reanalysis from the region to compare the distribution of mCDW across the two summers, and to explore the interannual variations with respect to wind and currents.

2 Data and methods

The CHINARE conducted comprehensive hydrographic surveys in the Amundsen Sea from the R/V *Xuelong* from 25 to 29 January, 2020 and 3 to 7 February, 2022. In this paper, data from 10 repeat CTD and Lowered Acoustic Doppler Current Profiler (LADCP) stations in the DGT is presented (Figure 1). The five stations observed along the trough are referred to as section A, and the five stations across the trough are referred to as section B. CTD data was collected using SBE-911 plus with an accuracy of 0.001 °C, and 0.0003 $S \cdot m^{-1}$ for temperature and conductivity, respectively.

Ocean currents were measured with a LADCP and a Ship (hull-mounted) Acoustic Doppler Current Profiler (SADCP). The LADCP was a 300 kHz RDI Workhorse Sentinel collecting data with an accuracy of ±5 $mm \cdot s^{-1}$. The LADCP data were processed using Matlab-based software from the Lamont Doherty Earth Observatory (version Ⅸ, Thurnherr, 2010). The SADCP data were obtained from a 38 kHz Ocean Surveyor on board the R/V *Xuelong*. The instrument was set to a bin thickness of 24 m with a total of 50 layers (the first layer at 34–50 m, and the final layer close to 1000 m). Given the bottom current velocity results are affected by the strong echo signal of the seafloor, the most effective observation depth on the continental shelf is at around 400 m. Therefore, in this paper we choose the 400 m planar current to analyze the deep current structure.

Tidal signals were removed from the SADCP and LADCP data using the Circum-Antarctic Tidal Simulation model (King et al., 2005). TS-MK-150 expendable bathythermographs (XBTs), which can observe temperature data to a depth of 760 m with an accuracy of 0.1 °C when the ship speed is 15 kn, were used to obtain temperature profiles at the shelf break in conjunction with the current observations at this location. Seal CTD temperature and salinity profile data in the Amundsen Sea (from February–March 2022) were downloaded from the Marine Mammals Exploring the Oceans Pole to Pole (MEOP) data portal (Roquet et al., 2014). The calibration procedure for the seal CTD data is described in Roquet et al. (2014), with the accuracy of data estimated to be within 0.03 °C for temperature and 0.05 for salinity, and a position error of within 1 km (Boehme et al., 2009). In this paper, only seal-CTD profiles with depths greater than 200 m are used.

The temperature and salinity properties of the water masses involved are shown in Table 1. In this paper potential temperature (θ) is used unless otherwise specified.

Table 1 Water mass characteristics of DGT

Water mass	Potential temperature (θ)/ °C	Salinity (S)	Reference
mCDW	θ>0	S>34.4	Biddle et al., 2017; Dotto et al., 2019
WW	θ<−1.5	S=~34.2	Miles et al., 2016
AASSW	θ>0	S<34	Miles et al., 2016

Since mCDW in this region is always bottom-intensified along the DGT, we define the 0 °C isotherm as the lower temperature boundary of mCDW. Accordingly, the changes in mCDW layer thickness and heat content presented refer to the water mass with temperatures above 0 °C.

Following the method of calculating the ocean heat content (Costa et al., 2008), the heat content of CDW (θ > 0 °C) Q_{mCDW} ($J \cdot m^{-2}$) was evaluated as:

$$Q_{\mathrm{mCDW}} = \int_{z_2}^{z_1} \rho C_{\mathrm{p}} (T - T_{\mathrm{fz}}) \mathrm{d}z \,, \tag{1}$$

where ρ is the *in situ* density ($kg \cdot m^{-3}$), C_{p} is the specific heat capacity of seawater ($J \cdot °C^{-1} \cdot kg^{-1}$), and T is the *in situ* temperature (°C). $T_{\mathrm{fz}} = -1.9$ °C is the *in situ* freezing point temperature. z_1 and z_2 represent the upper and lower bounds of the integrated depth layer (dbar).

Wind speeds used to examine the impact of wind variation on current and water mass property changes were obtained from the 0.25°×0.25° monthly average of the 10 m wind field data provided by European Centre for Medium-Range Weather Forecasts (ECMWF) Reanalysis 5 (Hersbach et al., 2018). The wind stress (τ) formula is as follows:

$$\tau = \rho_0 C_0 |V_{10}| V_{10} \,, \tag{2}$$

where ρ_0 =1.29 $kg \cdot m^{-3}$ is air density, C_0 is the drag coefficient between air and sea (Yin et al., 2007) and V_{10} is 10 m wind velocity ($m \cdot s^{-1}$).

The Ekman transport formula is as follows:

$$B = \frac{1}{f\rho} \tau \,, \tag{3}$$

where B is the volume transport, f is Coriolis parameter, and ρ =1027 $kg \cdot m^{-3}$ is the seawater density.

3 Result

3.1 Distribution of water masses in the DGT in 2020 and 2022

In this section, the distribution of water masses in the DGT are analyzed. Figure 2 shows that in both years the warm, fresh AASSW is limited to a very thin surface layer shallower than 50 m. The seasonal thermocline is located at 50–100 m, where the temperature decreases rapidly to below −1.5 °C and the salinity increases to above 34 (Figures 2a, 2b). WW characterized by the temperature minimum is mainly distributed between 100–300 m. The core temperature of WW is lower than −1.5 °C, with a minimum around −1.8 °C, approaching the *in situ* freezing point temperature (Figure 2c). The cooler temperature of the WW layer and the warmer temperature of the AASSW/mCDW above and below it produces a V-shaped structure in the θ–S diagram of the trough stations (Figure 2c). The mCDW with temperature above 0 °C is bottom-intensified below 400 m (Figure 2d). The mCDW layer is thickest at the southern end of the trough (close to 300 m), which is caused by the local topography and the mCDW from the northern DGT and BB ultimately converging here, albeit with a slightly cooler temperature.

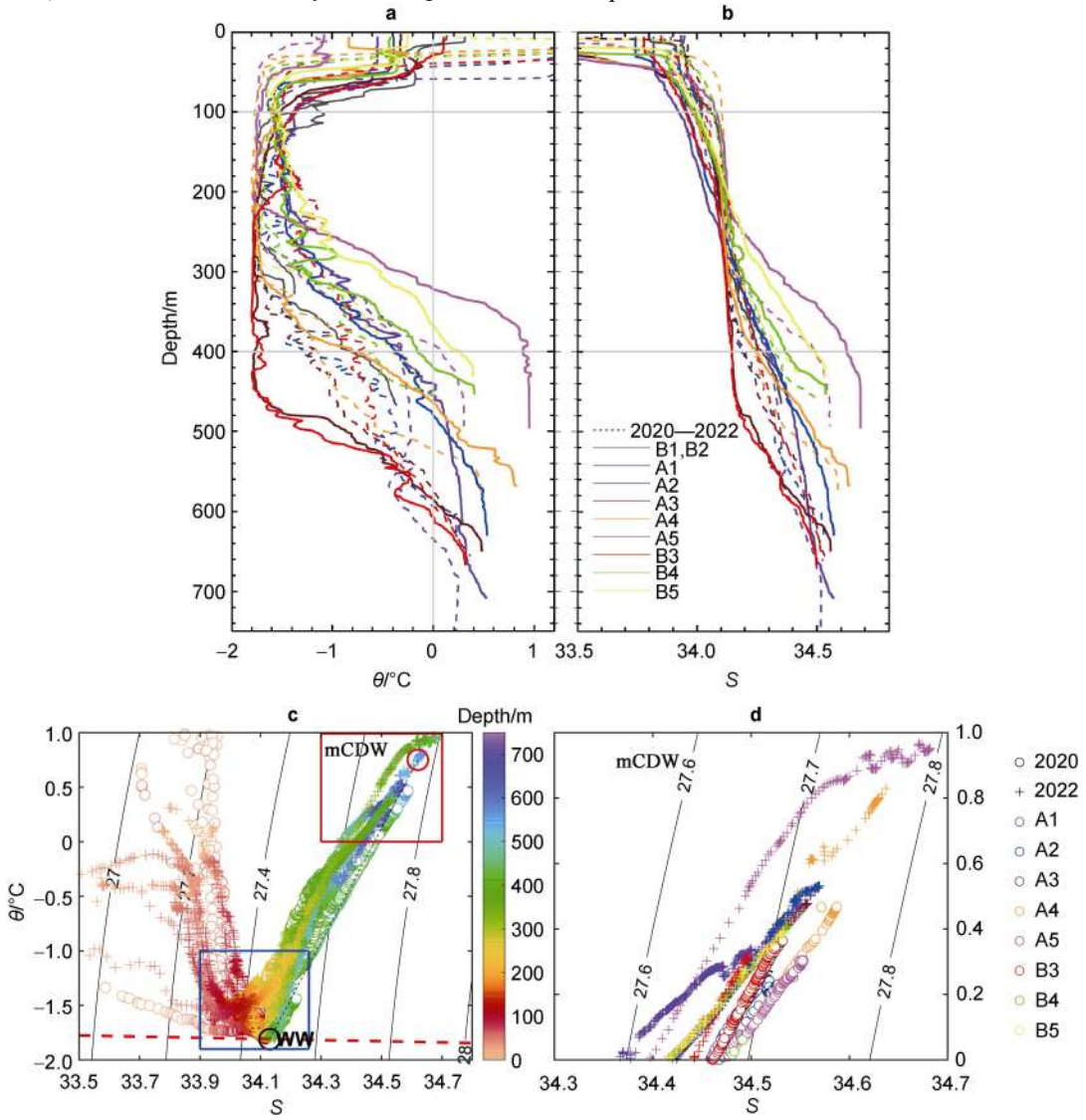

Figure 2 Vertical profiles and θ-S diagrams of all ship-based CTD stations. **a**, Vertical profiles of potential temperature (θ). The dotted lines represent 2020 observations, the solid lines represent 2022 observations, and the colors represent different stations. Gray vertical and horizontal lines represent the 100 m, 400 m isobath and 0 °C isotherm, respectively. **b**, Same as in (**a**) but for salinity. **c**, Open circles represent 2020 observations, and plus signs represent 2022 observations. The contours represent potential density (σ_θ), and red dashed line represents the surface freezing point. All data color-shaded for depth. The red and black circles represent the endpoint properties of mCDW and WW, respectively. The red and black boxes represent the approximate ranges of WW and mCDW, respectively. The black dashed line represents the line connecting the endpoints of WW and mCDW. **d**, Focused view of mCDW, colour-coded by CTD station locations.

Examining the stratification with vertical sections of water mass properties shows the bottom layers of section A, which extends from north to south along the trough, are occupied by warm and saline mCDW (Figures 3a–3c). The depth of the mCDW layer increases from about 400 m to over 700 m as the DGT deepens toward the shelf interior (Figures 3a and 3b). The upper boundary depth of WW also increased from about 10 m to over 100 m along the DGT, which is mainly influenced by the Amundsen Sea polynya and polar easterly winds. Section B crosses the middle of the DGT and the bank on each side (Figures 3b–3d). Here the mCDW entirely fills the bottom and is more concentrated on the eastern slope of the DGT. We note that mCDW was not observed on the western side of the DGT in either year, but was observed on the eastern side in 2022, in the bottom layer of stations B4 and B5 over BB.

Comparing the profiles from 2020 and 2022, the bottom temperature and salinity of the mCDW at most stations were significantly higher in 2022 (Figure 2). Along the bottom of the DGT, the maximum temperature in 2022 increases from 0.47 °C (A4) to 0.95 °C (A5), and the maximum salinity increases from 34.58 (A4) to 34.68 (A5).

3.2 Interannual variation of mCDW layer thickness

In addition to changes in salinity and temperature, there were also changes in the layer thickness/volume of the mCDW. Figures 3a and 3b shows that the mCDW layer (θ >0 °C) at the bottom of section A was thicker in 2022. The thickness of the mCDW layer in the DGT (Figure 3c) increases significantly at four stations along the north-south part of section A. At the southernmost stations, A1 and A2, the mCDW layer thickness more than doubles, increasing by 170 m and 118 m, respectively. Similarly in the north, the mCDW layer at stations A4 and A5 nearly doubled. For section B in 2020, there is only a weak presence of mCDW (15 m thick) at B4 on the east slope and complete absence of it at B5 above BB (Figure 3d). In 2022, the thickness of these two stations increases to 54 m and 60 m, respectively (Figure 3e). Overall there is a much larger distribution of mCDW at the bottom of BB in 2022 (Figure 3f).

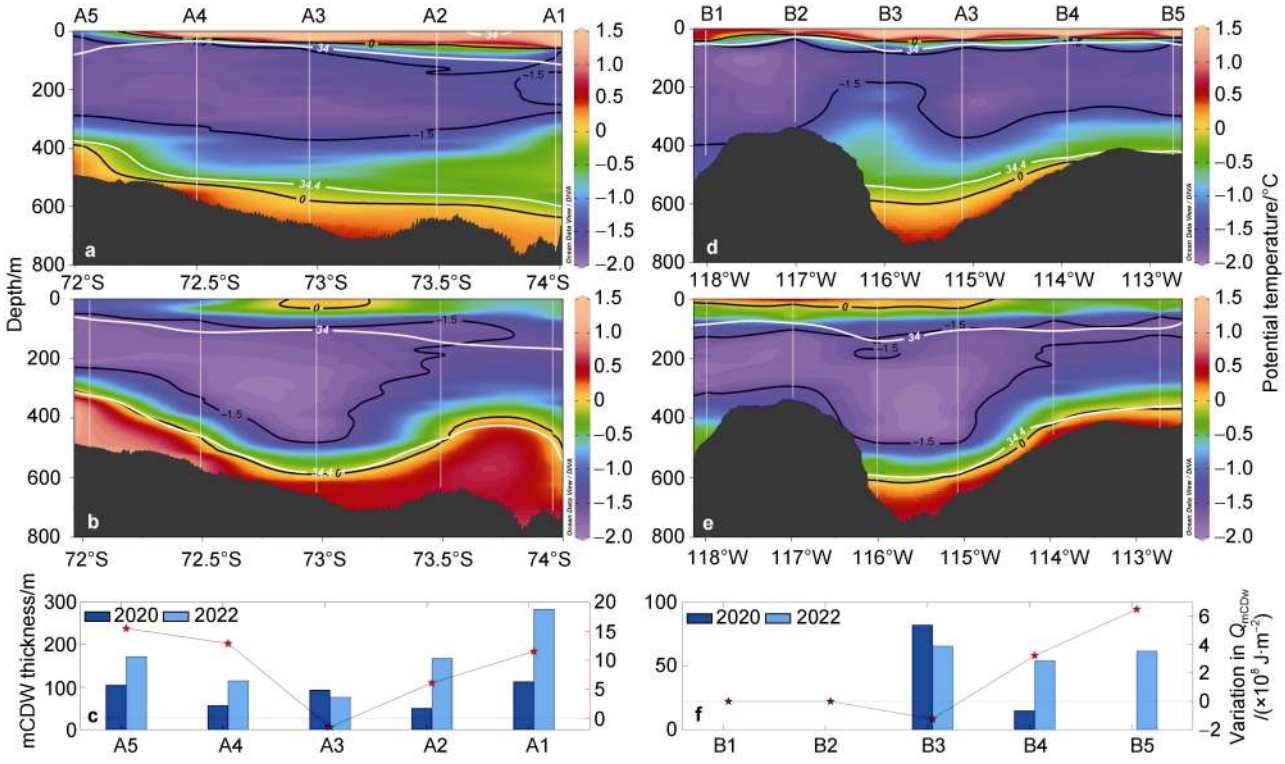

Figure 3 Vertical sections of potential temperature (θ) across section A (A1 to A5) for 2020 (**a**) and 2022 (**b**), and section B (B1 to B5) for 2020 (**d**) and 2022 (**e**). The temperature is color-shaded with black contours. White contours represent the salinity. The thickness of mCDW layer (blue bars) and mCDW heat content (red stars and dashed line) of section A (**c**) and section B (**f**). The plot was created with Ocean Data View (Schlitzer, 2018).

While there is a broad pattern of increased mCDW in 2022, with a doubling of the overall layer thickness and associated heat content (Figures 3c and 3f), a small decrease in mCDW thickness and heat content was observed in the middle of the trough at stations A3 and B3. The large increase in mCDW thickness at stations A1 and A2 in the southernmost part of the trough reinforces the significance of the decrease at stations A3 and B3 in the central region of the trough. This seems to indicate an eastward shift or expansion of the southward transport of mCDW in 2022. B1 and B2 on the west bank are always free of mCDW, which corresponds with previous studies. This is because

the inflow is mainly controlled by the local clockwise geostrophic current (Wåhlin et al., 2010).

3.3 General circulation of the DGT

In this section, the general circulation of water masses in the DGT are analyzed. From the previous section, mCDW is mainly distributed in the bottom layer below 400 m. The circulation at 400 m in Figures 4a and 4b shows that the mCDW flows southward through the north of the shallower trough, occupying the bottom layer below 400 m (Figure 3). In the south-central part of the trough (with depths below 600 m), the 400 m current is primarily northwestward, where mCDW flows southward along the deeper isobaths (Figure 3), and there is mainly outflow at 400 m. The current shifts southward at the southernmost point near the eastern side of the DIS.

In 2022, the current gradually turns from northeast to southeast (see blue arrows in Figure 4b) along the isobath from the shelf break into the northern part of the DGT. In addition, a strong eastward undercurrent was observed at 300–600 m entering the DGT from the shelf break in 2022 (Figure 4c). This is consistent with the movement and depth of warm CDW (about 1 °C) in Figure 4d. The undercurrent on the shelf break flows northeast along the isobath with velocity exceeding 25 cm·s^{-1}. After entering the trough across the shelf break at a depth about 500 m, the undercurrent gradually deflects along the direction of the trough. It shifts from eastward to southeastward, and finally turns southward, with its velocity decreasing below 20 cm·s^{-1}. The variation of the above-mentioned currents in the eastern part of the trough can be viewed as a part of a broad cyclonic circulation in the area. However, large interannual variations exist at the other locations in the trough.

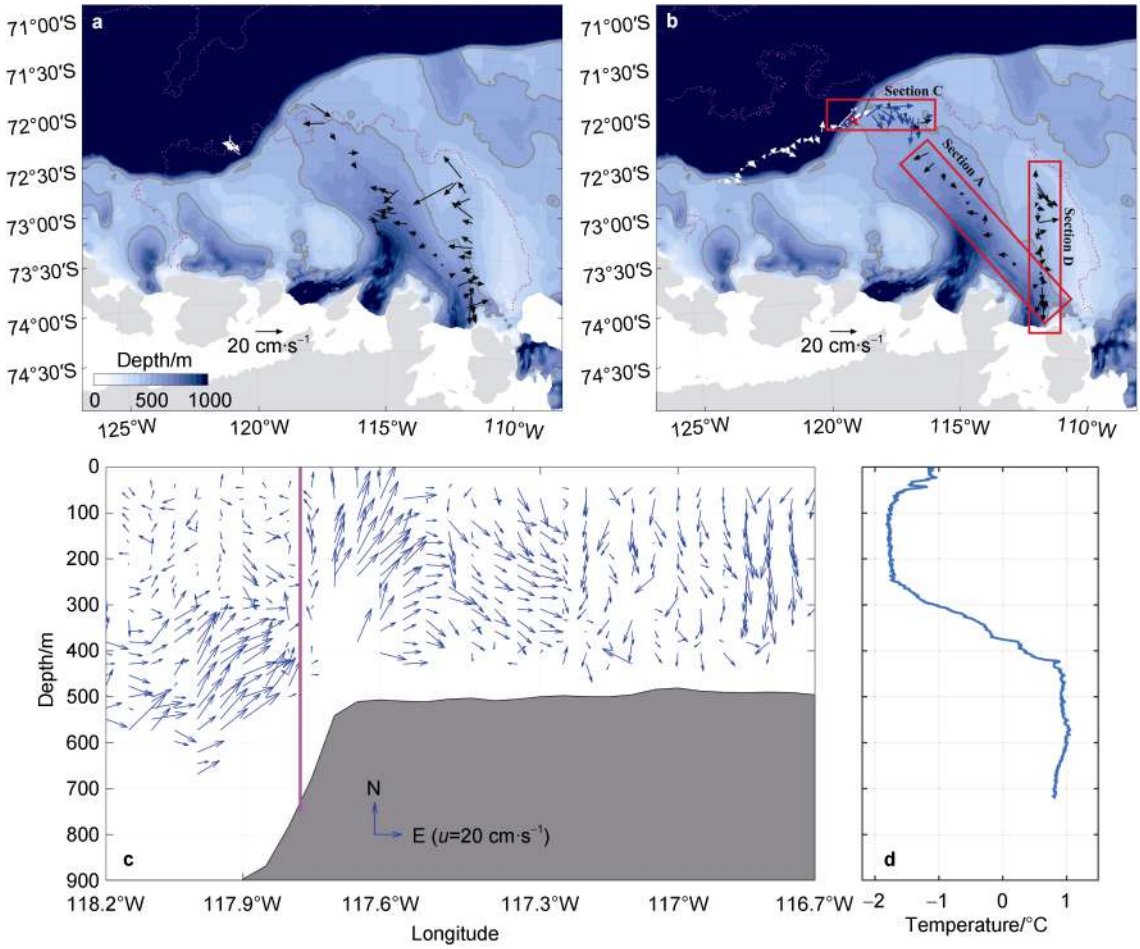

Figure 4 Average current field at 400 m in the DGT for 2020 (**a**) and 2022 (**b**). Bathymetry shading is the same as in Figure 1. The 600 m isobath is depicted by the grey line. White, blue and black arrows represent the currents on the continental slope and shelf break, respectively. The dashed magenta line represents the 30% sea ice concentration contour, noting the observation area is basically free of sea ice. **c**, Vertical section of ADCP current profiles in 2022 along section C (shown in Figure 4b). **d**, *In situ* temperature profile observed in 2022 at the station indicated by a red star in Figure 4b and the magenta line in Figure 4c.

3.4 Interannual variation of the circulation

In this section, the interannual variation of the circulation in the DGT is investigated. The 2020 observations on the northwest slope of the DGT (~120°W) reveal northwestward currents south of the slope and southwestward currents to the north (Figure 4a). In 2022, we observed eastward currents near the shelf at the same location (Figure 4b). When entering the shallower slope on the eastern side, the direction of the current changes to the northeast again along the extension of the isobath. The variation of the circulation at the same location can be seen more clearly from the vertical sections of current flow.

Compared to 2020, the southward flow in the bottom of the trough is strengthened in 2022. In 2020, the southward current was weak in the deeper layer between 72.4°S–72.8°S (Figure 5a). In contrast, the southward current was relatively stronger in 2022, and observed at depths deeper than 400 m with speeds of up to 15 cm·s^{-1} (Figure 5b). This corresponds to the thickening and warming of the mCDW layer in 2022 (Figure 2), indicating an intensification of mCDW flow into the trough. In 2020, a southward current with a speed of 10 cm·s^{-1} was observed in the bottom layer at a depth of 500 m at around 73.5°S, confirming that mCDW mainly flows southward at depth in this location, while the northward outflow is predominantly in the middle and upper layers of the trough.

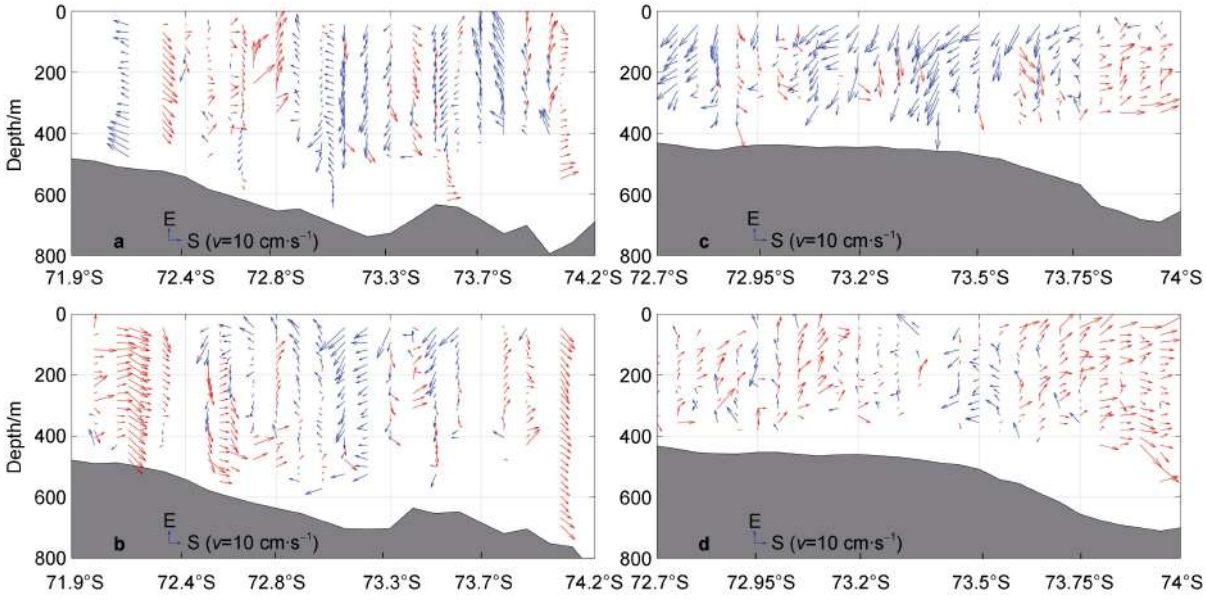

Figure 5 ADCP currents profiles along section A in 2020 (**a**) and 2022 (**b**), and along section D (shown in Figure 4b) in 2020 (**c**) and 2022 (**d**). Red (blue) arrows represent southward (northward) currents.

South of 73.7°S, the southward current in 2022 is relatively larger in extent and intensity. The southward current is also found to be dominant in the meridional observations from the southern end of the trough to the eastern BB (Figures 5c and 5d). In 2020, the BB was dominated by a northwestward outflow with more stable flow and increased speeds of around 20 cm·s^{-1} (Figure 5c). Conversely, the southward current is observed to have greater extent and intensity in 2022 (Figure 5d). A constant but slower northward current (~10 cm·s^{-1}) was only observed on the slope between the trough and the bank, while at the same time the southward current was less than 10 cm·s^{-1} on the bank, corresponding to the eastward shift in the distribution of mCDW distribution along the bottom in 2022 (Figure 2). In the following section we will examine the changes in circulation and mCDW transport relative to the wind regime in both years.

4 Discussion

The comparison of repeat hydrographic surveys in the DGT revealed a significant increase in the mCDW intrusion into the DGT in 2022, relative to 2020. Many studies have suggested that the variation of mCDW on the Amundsen Sea continental shelf is related to the variation of wind speed and direction (Dotto et al., 2019). Here we seek to elucidate the mechanism behind the observed changes between 2020 and 2022 by analyzing the zonal wind patterns in each year.

4.1 Mechanisms for enhanced mCDW inflows onto the continental shelf in 2022

Combining the wind data from the two years of observation reveals a significant southward shift of the meridional transition between easterly and westerly winds (Figure 6). Sometimes referred to as the Antarctic

Divergence (AD), this is a region of zero zonal wind stress. In the summer of 2019/20, the AD was over the basin area north of 71°S (Figures 6a–6d). In December 2019 the westerly winds were only in the northwestern corner of the sea area, when the entire Amundsen Sea was dominated by polar easterly winds (Figure 6a). In January 2020, the AD shifted southward, but overall the zonal winds on either side of the AD were weak (Figure 6b). By February, the AD had shifted once again to the basin north of 71°S (Figure 6c), when the southward current at the bottom of the trough was weakest (Figure 5a). In 2022 the AD stabilized around 72°S (Figures 6e–6h). In the eastern part of the Amundsen Sea AD moves onto the continental shelf and near the continental slope northwest of the DGT (Figure 6h), corresponding to the stronger southward current in the bottom of the trough (Figure 5b).

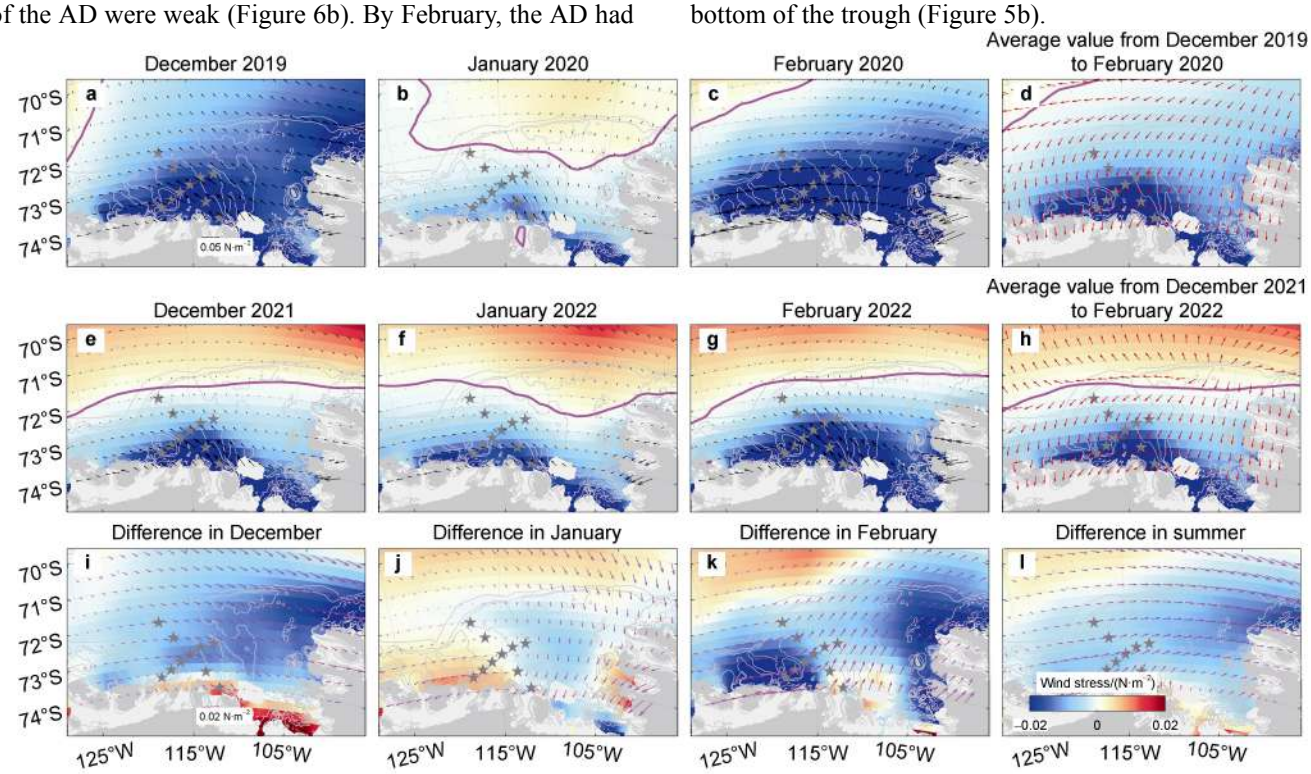

Figure 6 Wind stress (**a**–**h**) in the austral summer of 2020 and 2022, and their differences (**i**–**l**). Summer is defined from December of the previous year to February of the current year. Black arrows represent wind stress (**a**–**c**, **e**–**g**), red arrows represent sea surface Ekman transport direction (**d**, **h**), and magenta arrows represent the difference between two years of wind stress (**i**–**l**). Magenta lines indicate the zero-zonal-stress contour, also called the center of the AD.

The southward shift in the divergence zone promotes the flow of mCDW onto the continental shelf. The westerly/easterly winds north and south of the dividing line produces northward/southward Ekman transport in the upper layer of the ocean (Figures 6d and 6h), resulting in upwelling of deep CDW into the shallower layers and making it more accessible to the Amundsen Sea continental shelf (Figure 7). In summer 2022, the AD moves over the continental slope at the north of the DGT, therefore transporting more CDW from the bottom to depths shallower than 500 m (Figure 4d).

Stronger westerly winds over the continental slope strengthen the eastward undercurrent, increasing the transport of this CDW and its associated heat content to the DGT through Ekman dynamics (Wåhlin et al., 2012; Dotto et al., 2020). Compared with 2020, the westerly wind regime in the summer of 2022 is much further southward with its edge near the shelf break. This southward shift enhances the westerly winds at the continental slope, which in turn induces an increase/decrease in the sea level off-slope/near the coast. This change in the meridional gradient of sea level reportedly strengthens the eastward undercurrent (Dotto et al., 2020). A stronger undercurrent leads to an uplift of the isopycnals at the slope through Ekman dynamics (Wåhlin et al., 2012). When these isopycnals cross the shelf break, mCDW enters the DGT (Figure 7). Therefore, the increased westerly winds over the continental slope in 2022 is the primary mechanism driving the increased transport of mCDW to the DGT that year.

4.2 Eastward shift of the mCDW transport pathway during zonal wind enhancement

In 2022, when the mCDW inflows are enhanced, the path of the mCDW inflows into the DGT shifts eastward. The mCDW thickness decreases at stations B3 and A3, while it increases substantially at stations B4 and B5 in the east (Figure 3). Meanwhile, the bottom-of-dive properties

of the instrumented seal data in February–March 2022 revealed a large amount of mCDW on the east-side of BB (Figure 1) and a southward current is predominant in the south-central area of BB (Figure 5d). These results suggest that in 2022 the mCDW on the continental slope can directly access the shelf from BB in the northern part of the DGT.

The change of zonal wind direction sits on the shelf break just north of BB on the shelf break in 2022 (Figure 6), promoting the upwelling and southward transport of CDW to the shelf break. Thereafter the eastward undercurrent further assists the transport of mCDW directly from BB to the shelf (Figure 7) (Dotto et al., 2020). The mCDW on the BB is transported southeastward along the isobath (Figure 4b) and is limited by the shallower topography (< 300 m) in the middle of the bank. It eventually flows gradually southward from BB to the DGT. To the west, the divergence zone is further offshore of the continental slope (Figure 6). Accordingly, the mCDW directly entering the trough from the shelf break below 500 m on the west side of A5 does not increase, and even decreases at some locations (e.g. A3, B3). The increase in mCDW transported along the eastern bank explains the decreased mCDW at A3 and B3 in the central trough, together with the significant increase of A1 and A2 in the south.

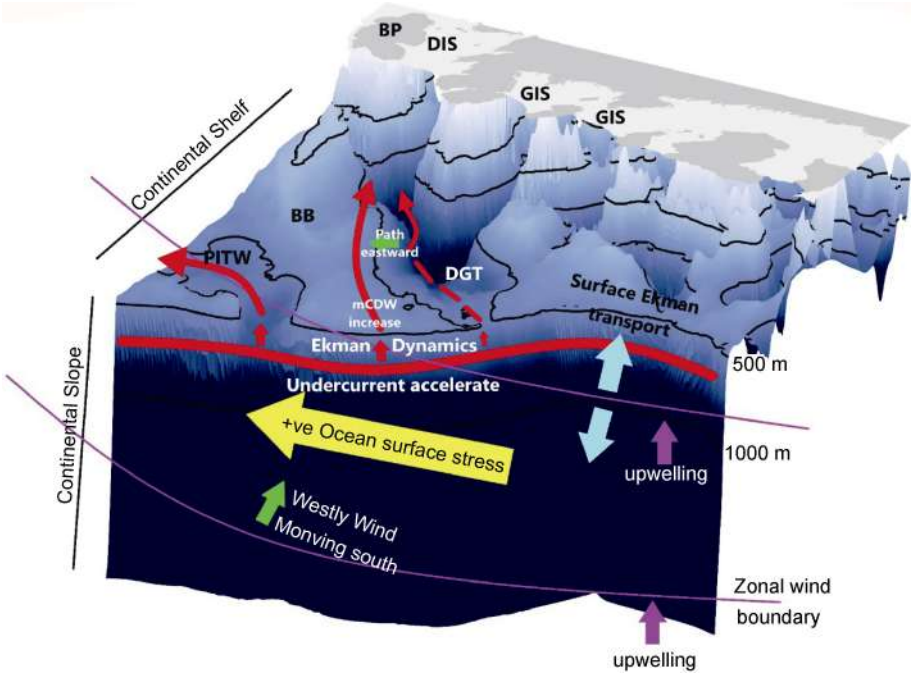

Figure 7 A schematic diagram of the processes underpinning the warmer shelf in 2022 and transport path eastward into the DGT. The process is described in discussion and conclusion sections. Bear Peninsula (BP), Getz Ice Shelf (GIS) and Pine Island Trough West (PITW) are indicated.

Finally, we acknowledge several caveats of our study. While the available ship-based observations within the DGT were sparse, the addition of a comprehensive amount of instrumented seal data in the 2022 season was invaluable. Overall our observations are in good agreement with the historical results. In addition, the variations we describe in the mCDW inflows to the DGT are limited to a very short time scale. In the future, we plan to study further the variability of mCDW inflows and glacial meltwater output over longer time scales by combining new mooring data, from the DGT with additional ship-based and instrumented seal data from other national programs.

5 Conclusion

In this paper, we presented the temperature, salinity and current velocity observations made by the CHINARE in the DGT during the summers of 2020 and 2022. Combined with instrumented seal data and a wind reanalysis over the same period, we showed the interannual variation of mCDW in the DGT and discussed the mechanisms underpinning it. Our findings are summarized as follows.

(1) The mCDW inflows is enhanced by the presence of a strong eastward undercurrent (up to 20 $cm \cdot s^{-1}$) on the continental slope to the north of the DGT.

(2) The mCDW inflows in the DGT are significantly enhanced in 2022 relative to 2020. We propose that in the summer of 2022 a southward shift in the westerly winds moved the upper oceanic divergence zone southward towards the continental shelf break, promoting the upwelling of mCDW above 500 m. Concurrently, the stronger westerly winds over the continental slope strengthened the eastward undercurrent, increasing the transport of this mCDW and its associated heat content to the DGT through Ekman dynamics.

(3) When the mCDW inflow is enhanced, its path

across the DGT moves eastward onto the BB. Conversely, when mCDW inflow is weak, mCDW will inflow mainly along the bottom of the trough below 500 m.

The observations show that there is strong interannual variation in the strength, path and extent of mCDW inflows to the DGT and that care must be taken when planning observation programs for long-term monitoring of the oceanic heat input to the ice shelves of this globally significant region.

Acknowledgements This study used data collected by the 36th and 38th CHINAREs, and we thank all the participants for their hard work. The marine mammal data were collected and made freely available by the International MEOP Consortium and the national programs that contribute to it (http://www.meop.net). This work is supported by Chinese Arctic and Antarctic Administration (Grant no. IRASCC2020-2022) and National Key R & D Program of China (Grant no. 2018YFA0605701). We thank Associate Editor Dr. Liyang Zhan and two anonymous reviewers, for reviewing this manuscript.

Availability of data and materials The monthly average 10 m wind field data can be found in European Centre for Medium-Range Weather Forecasts (ECMWF) Reanalysis 5 (ERA5; https://cds.climate.copernicus.eu/cdsapp#!/dataset/reanalysis-era5-single-levels-monthly-means?Tab=overview). Seal CTD temperature and salinity profile data can be found in Marine Mammals Exploring the Oceans Pole to Pole (MEOP; https://www.meop.net/database/download-the-data.html). Ship-based CTD, LADCP and SADCP data are available at Chinese National Arctic and Antarctic Data Center (http://www.chinare.org.cn).

References

Arneborg L, Wåhlin A K, Björk G, et al. 2012. Persistent inflow of warm water onto the central Amundsen shelf. Nat Geosci, 5(12): 876-880, doi:10.1038/ngeo1644.

Biddle L C, Heywood K J, Kaiser J, et al. 2017. Glacial meltwater identification in the Amundsen Sea. J Phys Oceanogr, 47(4): 933-954, doi:10.1175/jpo-d-16-0221.1.

Boehme L, Lovell P, Biuw M, et al. 2009. Technical Note: animal-borne CTD-Satellite Relay Data Loggers for real-time oceanographic data collection. Ocean Sci, 5(4): 685-695, doi:10.5194/os-5-685-2009.

Costa D P, Klinck J M, Hofmann E E, et al. 2008. Upper ocean variability in west Antarctic Peninsula continental shelf waters as measured using instrumented seals. Deep Sea Res Part II Top Stud Oceanogr, 55(3/4): 323-337, doi:10.1016/j.dsr2.2007.11.003.

Dotto T S, Naveira Garabato A C, Bacon S, et al. 2019. Wind-driven processes controlling oceanic heat delivery to the Amundsen Sea, Antarctica. J Phys Oceanogr, 49(11): 2829-2849, doi:10.1175/jpo-d-19-0064.1.

Dotto T S, Naveira Garabato A C, Wåhlin A K, et al. 2020. Control of the oceanic heat content of the Getz-Dotson Trough, Antarctica, by the Amundsen Sea low. J Geophys Res Oceans, 125(8): 1-19, doi:10.1029/2020jc016113.

Dutrieux P, De Rydt J, Jenkins A, et al. 2014. Strong sensitivity of Pine Island ice-shelf melting to climatic variability. Science, 343(6167): 174-178, doi:10.1126/science.1244341.

Hersbach H, Bell B, Berrisford P, et al. 2018. ERA5 hourly data on single levels from 1979 to present, Copernicus Climate Change Service (C3S) Climate Data Store (CDS). [2022-05-05]. https://cds.climate.copernicus.eu/cdsapp#!/dataset/reanalysis-era5-single-levels?tab=overview.

Jenkins A, Dutrieux P, Jacobs S S, et al. 2010. Observations beneath Pine Island Glacier in West Antarctica and implications for its retreat. Nat Geosci, 3(7): 468-472, doi:10.1038/ngeo890.

Joughin I, Smith B E, Medley B. 2014. Marine ice sheet collapse potentially under way for the Thwaites Glacier Basin, West Antarctica. Science, 344(6185): 735-738, doi:10.1126/science.1249055.

Kim T W, Ha H K, Wåhlin A K, et al. 2017. Is Ekman pumping responsible for the seasonal variation of warm circumpolar deep water in the Amundsen Sea? Cont Shelf Res, 132: 38-48, doi:10.1016/j.csr.2016.09.005.

Kim T W, Yang H W, Dutrieux P, et al. 2021. Interannual variation of modified circumpolar deep water in the Dotson-Getz Trough, West Antarctica. J Geophys Res Oceans, 126(12): e2021JC017491.

King M, Penna N, Clarke P. 2005. Validation of ocean tide models around Antarctica using onshore GPS and gravity data. J Geophys Res Atmos, 110(B8): B08401, doi:10.1029/2004JB003390.

Miles T, Lee S H, Wåhlin A, et al. 2016. Glider observations of the Dotson Ice Shelf outflow. Deep Sea Res Part II Top Stud Oceanogr, 123: 16-29, doi:10.1016/j.dsr2.2015.08.008.

Mouginot J, Rignot E, Scheuchl B. 2014. Sustained increase in ice discharge from the Amundsen Sea Embayment, west Antarctica, from 1973 to 2013. Geophys Res Lett, 41(5): 1576-1584, doi:10.1002/2013gl059069

Nakayama Y, Menemenlis D, Zhang H, et al. 2018. Origin of Circumpolar Deep Water intruding onto the Amundsen and Bellingshausen Sea continental shelves. Nat Commun, 9(1): 3403, doi:10.1038/s41467-018-05813-1.

Pritchard H D, Ligtenberg S M, Fricker H A, et al. 2012. Antarctic ice-sheet loss driven by basal melting of ice shelves. Nature, 484(7395): 502-505, doi:10.1038/nature10968.

Roquet F, Williams G, Hindell M A, et al. 2014. A southern Indian Ocean database of hydrographic profiles obtained with instrumented elephant seals. (2022-05-15). Sci Data 1: 10. https://doi:10.1038/sdata.2014.28.

Schlitzer R. 2018. Ocean Data View. [2021-05-10]. http://odv.awi.de.

St-Laurent P, Klinck J M, Dinniman M S. 2013. On the role of coastal troughs in the circulation of warm Circumpolar Deep Water on Antarctic shelves. J Phys Oceanogr, 43(1): 51-64, doi:10.1175/jpo-d-11-0237.1.

Sutterley T C, Velicogna I, Rignot E, et al. 2014. Mass loss of the Amundsen Sea Embayment of West Antarctica from four independent techniques. Geophys Res Lett, 41(23): 8421-8428, doi:10.1002/2014gl061940.

Thoma M, Jenkins A, Holland D, et al. 2008. Modelling circumpolar deep water intrusions on the Amundsen Sea continental shelf, Antarctica. Geophys Res Lett, 35(18): L18602, doi:10.1029/2008gl034939.

Thurnherr A M. 2010. A practical assessment of the errors associated with full-depth LADCP profiles obtained using teledyne RDI workhorse acoustic Doppler Current profilers. J Atmos Ocean Technol, 27(7): 1215-1227, doi:10.1175/2010jtecho708.1.

Turner J, Orr A, Gudmundsson G H, et al. 2017. Atmosphere-ocean-ice interactions in the Amundsen Sea Embayment, West Antarctica. Rev

Geophys, 55(1): 235-276, doi:10.1002/2016rg000532.

Wåhlin A K, Yuan X, Björk G, et al. 2010. Inflow of warm circumpolar deep water in the central Amundsen shelf. J Phys Oceanogr, 40(6): 1427-1434, doi:10.1175/2010jpo4431.1.

Wåhlin A K, Muench R D, Arneborg L, et al. 2012. Some implications of Ekman layer dynamics for cross-shelf exchange in the Amundsen Sea. J Phys Oceanogr, 42(9): 1461-1474, doi:10.1175/jpo-d-11-041.1.

Walker D P, Brandon M A, Jenkins A, et al. 2007. Oceanic heat transport onto the Amundsen Sea shelf through a submarine glacial trough. Geophys Res Lett, 34(2): L02602, doi:10.1029/2006gl028154.

Walker D P, Jenkins A, Assmann K M, et al. 2013. Oceanographic observations at the shelf break of the Amundsen Sea, Antarctica. J Geophys Res Oceans, 118(6): 2906-2918, doi:10.1002/jgrc.20212.

Yin X B, Wang Z Z, Liu Y G, et al. 2007. Ocean response to Typhoon Ketsana traveling over the northwest Pacific and a numerical model approach. Geophys Res Lett, 34(21): L21606, doi:10.1029/2007gl031477.